



OPEN CFD-enabled sustainable design and manufacturing of cooling fan for unmanned helicopter

Liang Si^{1,2}, Zhixin Liu¹✉, Nannan Xiao¹, Yuwen Zhang¹, Yebao Liu¹, Shuai Deng¹, Yuchuan Li¹, Haisheng Yang¹, Xiongjian Zhang¹, Guoqiang Fu¹ & Joon Phil Choi^{3,4}✉

Due to the demand of unmanned helicopters for drag reduction and rain-proof, the helicopter nacelle must be sealed. It will lead to a decrease in the heat transfer efficiency of the radiator, and the output power of the engine will drop dramatically. The helicopter's flight safety will be seriously jeopardized, especially when the helicopter is hovering (maximum engine power is needed). Currently, active cooling by equipping the radiator with a fan is the only solution, and the heat transfer efficiency of the radiator could be controlled by fan. Therefore, the performance of the fan directly affects the flight safety of the whole system. In this study, the Airfoils 30, suitable for low Reynolds number flows, is adopted to design the fan blade considering the characteristics of helicopter heat sink miniaturization and high integration. Then, a three-dimensional CFD (computational fluid dynamics) k- ω SST model is developed to investigate the effects of fan blade torsion angle, chord length, mounting angle and the number of blades on the performance of the fan. Furthermore, the constraints of radiator dimension, air flow resistance on the performance of the fan are considered comprehensively to finalize the new fan configuration. The optimised parameters of fan suitable for high flow rate (above 1.17 kg/s) are chord length is 55 mm, torsion angle is 26°, mounting angle is 39° and the blade number is 7. The fan efficiency increases about 13.6%. The power consumption decreases about 9.5% (about 73 W). The fan rotational speed decreases 10.5%. The improvement of fan efficiency is a key measure for energy conservation and carbon reduction in unmanned helicopter systems. The 73 W power consumption of the fan decrease indicates that 1.2 kg green-house gas emission reduces per day. The lower power consumption will result in a 0.14% cruising endurance increase. The fan is then manufactured by additive manufacturing based on CFD optimization results. This deep integration between CFD and additive manufacturing reduces trial and error costs and energy consumption. It also shows the promising future of UAV components autonomous manufacturing. Finally, the experiment is conducted in lab under 40°C. The experimental results indicate that the maximum output power of the engine is over than 90 kW. Based on the helicopter main rotor performance curve, the helicopter could hover indefinitely with 500 kg loading under 40 °C. It is a criterion to identify the designing success.

Keywords Unmanned helicopter, CFD simulation, Fan design, Additive manufacturing, Performance curve

The helicopter cooling system is critical in determining the hovering time and maximum load capacity of the unmanned helicopter system. Existing cooling system mainly consists of water-cooled radiators, air-cooled radiators, fans, motors, etc. The radiators are of body-mounted design, with the outer contour aligned with the fuselage contour to reduce the drag force during flight, and internally connected to the fan through the air intake ducts. The size of the radiator should be small and lightweight enough to ensure, that the unmanned helicopter can take off under plateau. Additionally, the engine over-heat phenomenon may happen as the helicopter hovers due to the high air temperature, which seriously affects the power output of the engine and the safety of Unmanned helicopter. Therefore, subject of the layout limitations of avionics equipment inside the fuselage and its own loading, it is necessity to optimize the design of the existing fan to achieve the purpose of improving the cooling efficiency of the cooling system. Finally, the balance between fan efficiency and the size should be made intentionally.

¹Aerospace Times Feihong Technology Company Limited, Beijing, China. ²National Elite Institute of Engineering, Northwestern Polytechnical University, Xi'an, China. ³Department of 3D Printing, Korea Institute of Machinery & Materials, Daejeon, Republic of Korea. ⁴School of Mechanical Engineering, Chung-Ang University, Seoul 06974, Republic of Korea. ✉email: Liuz0053@e.ntu.edu.sg; jpchoi@kimm.re.kr

Currently, there are two main categories for studying the performance of fans: experimental and numerical methods¹. Experimental methods require high accuracy of the environment, test setup, test conditions, and test samples, so they are more costly, time-consuming, and less reproducible. Numerical methods depend on the principle of CFD (Computational fluid dynamics). The continuity equation, Navier–Stokes equations and turbulence models are solved to obtain the detailed flow information within the flow field. Nowadays, with the development of computer technology, CFD simulation technology has been widely used. Many good results in fans design have been obtained by the scholars. Initially, S. Moreau et al. applied CFD technology to analyze the flow field inside the fan, and obtained satisfactory results in a limited time². Then significant results have been achieved in related fields^{3–10}. Li Shengfu et al. investigated the effects of the following factors on the performance of automotive fans in terms of blade selection¹¹, number of blades¹², hub ratio¹³, and blade mounting angle¹⁴, respectively. The results of the investigations show that the blade airfoil should be identified based on the Mach number of the airflow on the blade surface. As the fan configuration and the working conditions keeping unchanged, the air flow rate and efficiency of the fan gradually increase with the increase in the number of blades, but the increase in the flow rate and efficiency is smaller when the number of blades is increased to seven and above^{15,16}. It is due to the friction between air and the fan blade. The flow rate of the fan increases significantly with a slightly increase in the mounting angle of the blades while the efficiency of the fan decreases with an increase in the mounting angles^{15,16}. Ye Li's study showed that the effect of hub ratio on the efficiency is not clear¹⁵, while Tang Zhao's study showed that the flow rate of the fan decreases with increasing hub ratio¹⁶. Smaller hub ratios is beneficial for improving the aerodynamic performance of the fan but it should be noted that higher fan blade strength is required as well, which will lead to more difficulty of manufacturing.

The drag force of the helicopter is composed of parasitic drag force, induced drag force and airfoil drag force and affects the performance of the helicopter significantly^{17,18}. The parasitic drag force is caused by the fuselage, landing gear and the rotor hub. It is proportional to the square of the helicopter air speed. Hence, the parasitic drag force can be omitted as the helicopter is hovering. The largest induced drag force appears as the helicopter is hovering. The air flow direction is changed suddenly by the main rotor. However, the induced drag force drops significantly as the helicopter starts moving. The airfoil drag force which is proportional to the air velocity is caused by the airfoil resistance and the friction between rotor and air. The airfoil drag force changes slightly due to the comprehensive effects of main rotor and the tail rotor under medium velocity conditions. In all, the highest drag force of the helicopter system occurs as the helicopter is hovering. The high engine power and the cooling system heat load occur simultaneously. Because of that, active cooling is the only solution for cooling system as the helicopter is hovering. High performance fan is crucial for the Unmanned helicopter system.

In summary, the mentioned above investigations on fans are notable and beneficial for the future fan design. However, the requirements of fan miniaturization, lightweightness and high integration are relatively urgent due to the space limitations and load requirements of the helicopter. There is a research gap in systematical investigation of the small size, high flow rate fans used for unmanned helicopter. According to the working environment of helicopter fan, this paper firstly identifies the fan blade airfoil type based on the estimated mass flow rate and air velocity on the blade surface, and then a three-dimensional CFD model k-omega SST is developed. Furthermore, the fan parameters, such as torsion angle, chord length, mounting angle, and number of blades are studied and optimized thoroughly. The simulation results show that the optimized fan efficiency increases about 13.6%. The power consumption decreases about 9.5% (about 73 W). The fan rotational speed decreases 10.5% as compared to the original one used in the lab now. The optimized fan is manufactured by additive manufacturing method for the keeping the product accuracy. Finally, the experiments are conducted in the lab. The experimental results show that maximum output power of the engine is over than 90 kW under 40°C. It indicates that the helicopter can hovering indefinitely with 500 kg loading under 40°C.

In summary, previous investigations on fan performance have provided valuable insights; however, the miniaturization, lightweight design, and high integration requirements of unmanned helicopters pose new challenges. There remains a clear research gap in systematical studying high compact, high-flow-rate fans specifically tailored for Unmanned helicopter cooling systems. This study addresses that gap by identifying an appropriate blade airfoil type under low Reynolds number conditions firstly, followed by developing a validated three-dimensional CFD k-omega SST model to optimize critical fan parameters, such as torsion angle, chord length, mounting angle, and blade number. The optimized fan is then fabricated using additive manufacturing to ensure precision and repeatability, and its performance is experimentally validated.

Furthermore, this work contributes to the broader context of the manufacturing for Sustainable Industry initiative. Sustainability is supported through the use of additive manufacturing, which enables complex geometries with reduced material waste and improved resource efficiency^{19,20}. Manufacturing potential is demonstrated by integrating CFD-based design optimization with additive manufacturing^{21,22}, establishing a foundation for future CFD based design and closed-loop cyber-physical production systems. Broader impact is expected, as the presented methodology and digital-manufacturing framework can be extended beyond UAV cooling fans to other aerospace and industrial components, advancing the vision of sustainable manufacturing systems.

Numerical modeling and experimental validation

The framework of this study is shown in figure below (Fig. 1). It can be summarized as follow:

Phase I: the CFD model is developed by coupling continuity equation, momentum equation and turbulence models based on the Unmanned helicopter requirements.

Phase II: The numerical model is validated by the experiments, and then configuration is optimized comprehensively by considering the torsion angle, chord length, mounting angle, and number of blades.

Phase III: The product is fabricated by additive manufacturing based on the optimized parameters. Then the cooling fan is adopted to check the system matching in the application.

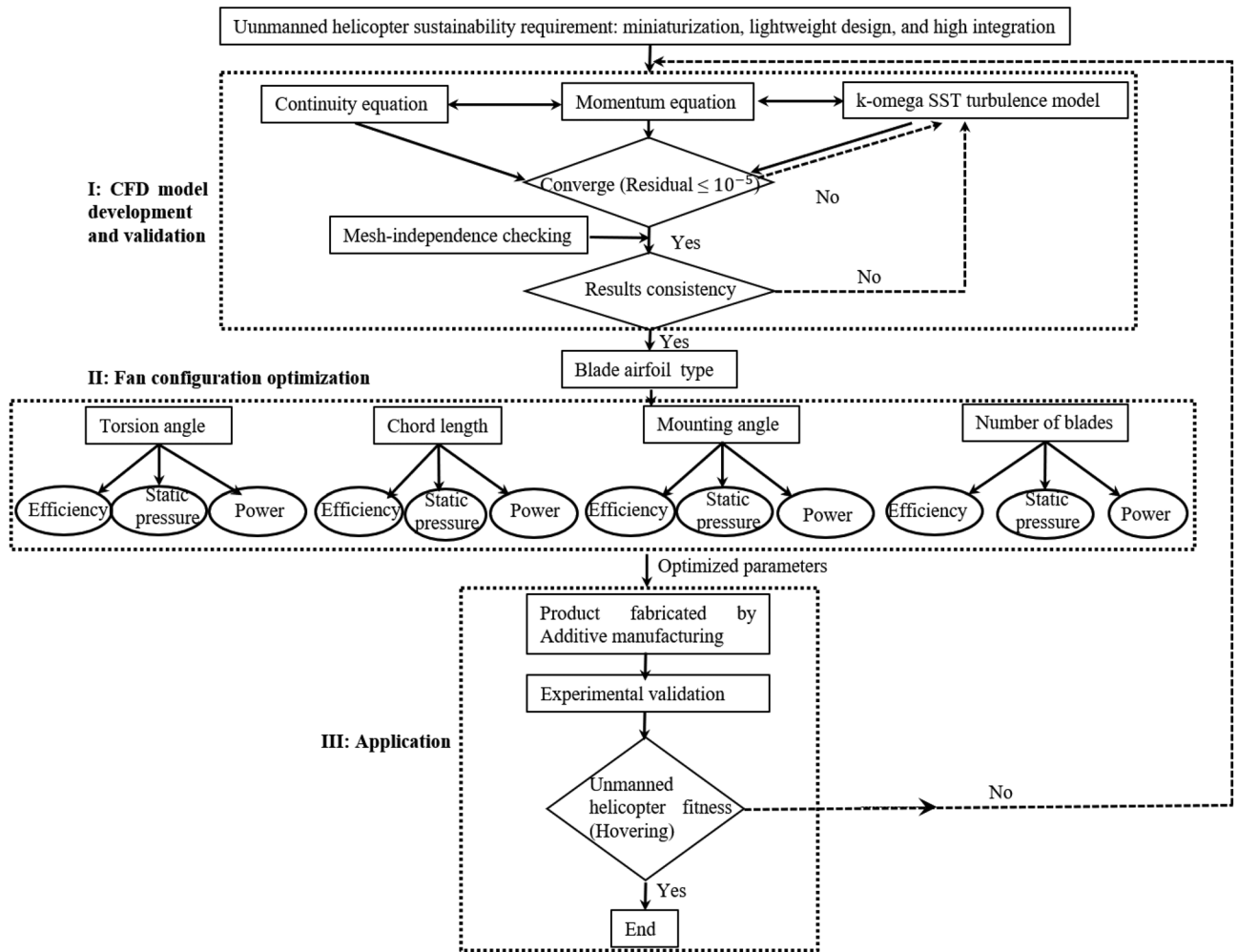


Fig. 1. Flow chat of CFD enabled sustainable design and manufacturing of cooling Fan for unmanned helicopter.

Numerical modeling

The team’s existing helicopter system has been configured with a fan (the original one). The number of blades of the fan is 7. In order to design a new fan with better performance using CFD, the original one is firstly investigated thoroughly. The specific modeling process is shown below. The computational fluid zone is divided into the enter zone, the rotating zone and the exit zone. The radius of the air inlet and outlet is 700 mm. The distance from the rotating domain of the fan to the inlet is 700 mm. In order to capture the detailed information near the blades, the fine meshes near the leading and trailing edges of the blades are created, and the distribution of meshes of the entire model is shown in (Fig. 2).

Governing equations

CFD has been adopted in various areas to examine the fluid behavior. Due to the low Mach number of the fluid, the incompressible fluid model is adopted to evaluate the velocity, pressure distribution. By solving the mass conservation equation, momentum equation, and the k-omega SST model, the converged fluid flow parameters distribution, such as fluid pressure and velocity is obtained.

The incompressible mass conservation equation is^{23,24}

$$\frac{\partial U_i}{\partial x_i} = 0 \tag{1}$$

The conservation of momentum is

$$\rho \frac{\partial U_i}{\partial t} + \rho U_j \frac{\partial U_i}{\partial x_j} = \frac{\partial P}{\partial x_i} + \mu \frac{\partial}{\partial x_i} \frac{\partial}{\partial x_j} U_i + \frac{\partial}{\partial x_i} \left[\mu_\tau \frac{\partial U_i}{\partial x_j} + \frac{\partial U_j}{\partial x_i} \right] \tag{2}$$

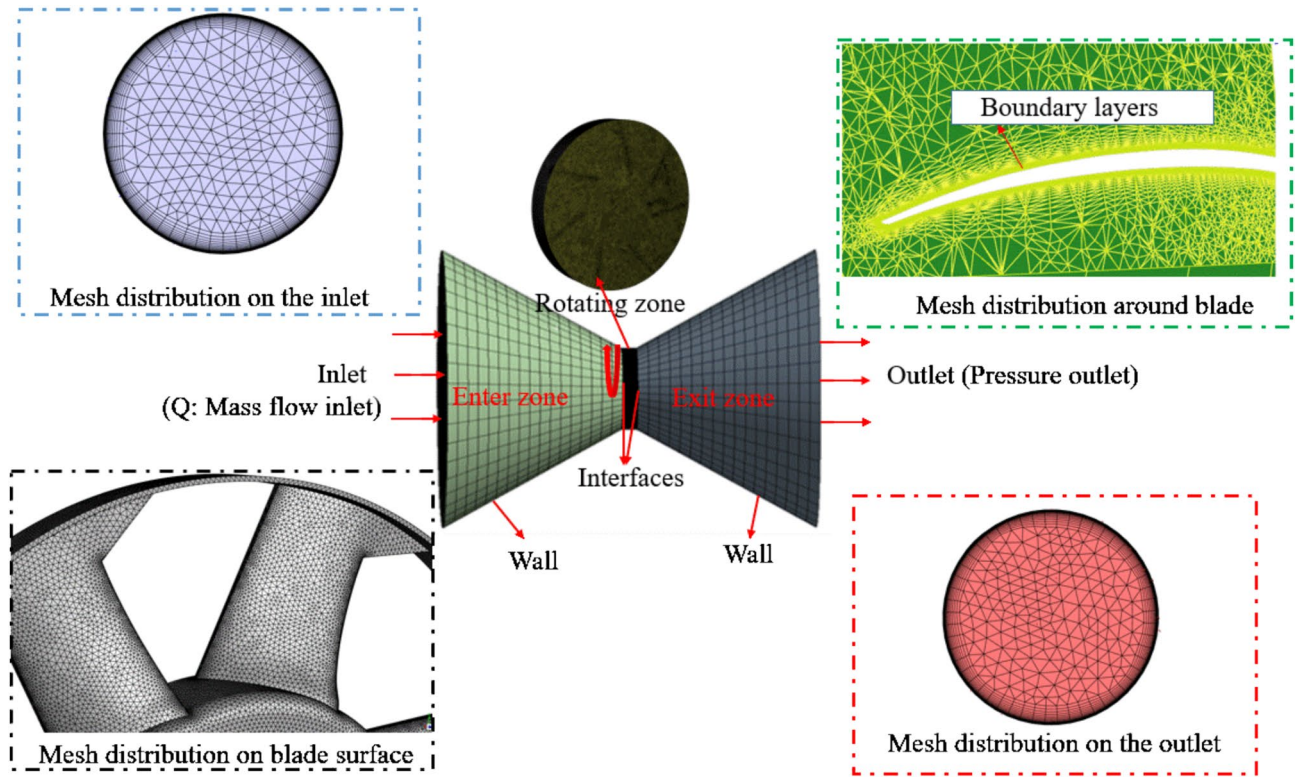


Fig. 2. Overall mesh division of computational domain.

where: P (Pa) is the fluid static pressure; U_i, U_j (m/s) is the mean velocity component; x_i, x_j is the coordinate component; μ is the kinetic viscosity coefficient (Pa.s); μ_t is the turbulent viscosity coefficient.

The k-omega SST turbulence model is defined by two equations: energy Eq. (3) and dissipation equation: (4).

The k- ω turbulence model is

$$\frac{\partial(\rho k)}{\partial t} + \nabla \cdot (\rho U k) = \nabla \cdot [(\mu + \sigma_k \mu_t) \nabla k] + \frac{\partial U_j}{\partial x_i} + P_k - \beta^* \rho \omega k \tag{3}$$

$$\frac{\partial(\rho \omega)}{\partial t} + \nabla \cdot (\rho U \omega) = \nabla \cdot [(\mu + \sigma_\omega \mu_t) \nabla \omega] - \alpha \frac{\omega}{k} P_k - \beta \rho \omega^2 + 2(1 - F_1) \rho \sigma_{\omega 2} \frac{1}{\omega} \nabla k \cdot \nabla \omega \tag{4}$$

$$\mu_t = \frac{\rho k}{\omega} \cdot \frac{a_1}{\max(a_1, \Omega F_2)} \tag{5}$$

$$\Omega = \sqrt{\Omega_{ij} \Omega_{ij}} \tag{6}$$

$$P_k = \mu_t (\nabla U + (\nabla U)^T : \nabla U) \tag{7}$$

$$F_1 = \tanh \left(\left\{ \min \left[\max \left(\frac{\sqrt{k}}{\beta^* \omega y}, \frac{500 \gamma}{y^2 \omega} \right), \frac{4 \rho \sigma_{\omega 2} k}{CD_{k\omega} y^2} \right] \right\}^4 \right) \tag{8}$$

$$CD_{k\omega} = \max \left(2 \rho \sigma_{\omega 2} \frac{1}{\omega} \frac{\partial k}{\partial x_i} \frac{\partial \omega}{\partial x_i}, 10^{-10} \right) \tag{9}$$

$$F_2 = \tanh \left(\left[\max \left(\frac{2 \sqrt{k}}{\beta^* \omega y}, \frac{500 \gamma}{y^2 \omega} \right) \right]^2 \right) \tag{10}$$

where U_i, U_j (m/s) is the mean velocity component; x_i, x_j is the coordinate component; $\beta^* = 0.09$, $\sigma_{k1} = 0.85$, $\sigma_{k2} = 1$, $\sigma_{\omega 1} = 0.5$, $\sigma_{\omega 2} = 0.856$, $a_1 = 5/9$, $a_2 = 0.44$, $\beta_1 = 3/40$, $\beta_2 = 0.0828$. $\sigma_{\omega 1}, \sigma_{k1}$ denotes the zone near the wall. $\sigma_{\omega 2}, \sigma_{k2}$ denotes the zone away from the wall.

Boundary conditions

The air is modeled as fluid in the simulation. The air density is 1.225 kg/m^3 , and the dynamic viscosity is $1.716 \times 10^{-1} \text{ Pa}\cdot\text{s}$. The turbulence model used in the simulation is k- ω SST model. The wall is modeled as static wall. The air inlet flow rate is 1.17 kg/s , and the model outlet is normal atmosphere pressure (20°C , and 101.3 Kpa). The rotating speed of the fan is 4250 RPM . The coupled pressure–velocity solution method is a second-order upwind algorithm. The interfaces between the entre, exit zone and the rotating zone are modelled as interface to ensure the convergence of the model.

Verification of mesh-independence

The mesh distribution strategy has a great impact on the accuracy of numerical solution. In CFD simulation, the mesh is usually refined in the key flow area to capture the critical behavior of the fluid. The blade leading and trailing edges are refined in this study. The mesh size is adjusted appropriately in the area of no-interested (enter zone and exit zone in this study). A reasonable grid parameter control strategy is adopted in this study to keep the balance between the numerical results accuracy and the cost. y^+ is critical in simulation. If the y^+ is too small, the calculation would be costly. If the y^+ is too large, the detailed information near the wall cannot be captured. The first layer of the boundary layers (20 layers) is set at $4.5 \times e^{-6} \text{ m}$ to ensure $y^+ \approx 1$. To test the mesh independency, the growth rate of the mesh is varied from 1.15, 1.18 to 1.20. The minimum and maximum mesh size are set as 0.001 m and 0.1 m , respectively. The adaptive sizing strategy is adopted. The curvature angle normal angel is 18° . Cell target skewness is set as 0.9. The total volume mesh is about three million, two million and one million, respectively.

In this research, the air flow rate of 1.17 kg/s , fan rotational speed of 4750 RPM , temperature of 20°C , and working pressure of atmosphere (101.3 Kpa) are selected for mesh-independent validation. The Ansys fluent meshing is adopted to generate the mesh automatically. Then numerical calculations are carried out under the same working conditions, and the fan performance is obtained under three different mesh quantities. The results are shown in (Fig. 3). The mass flow rate refers to the air entering from the inlet and exiting from outlet. The static pressure refers to the static pressure difference between the fan inlet and outlet interface. The fan performance curves almost coincide with the three different grid conditions. Hence, the number of meshes is constrained within one million to save the computational resources and time.

Validation of numerical model

In this study, the experimental data obtained from the manufacture is adopted to validate the numerical model²⁵. The comparison between the numerical results and experimental results are shown in (Fig. 4). The experimental results are consistent with the simulation results. It indicates that the CFD numerical model is reliable to do the multi-factor investigations. Similar methods have been adopted by scholars in their investigations and valuable results have been obtained^{26,27}. In the next section, the impacts of blade torsion angle, chord length, mounting angle, and number of blades on the fan performance will be elaborated.

Fan design optimization

In this study, ‘optimization’ denotes a discrete parametric screening (predefined levels) and selection of the best candidate among the evaluated design points, rather than a continuous iterative optimization loop or Pareto-front analysis. The discrete increments (e.g., integer-degree angles) were chosen to control computational cost and to maintain practically manufacturable/adjustable blade settings.

Identification of fan blade airfoil type

Due to the structural and weight limitations of the helicopter, the cooling system is miniaturized and high integrated, which results in a high resistance when the cooling air flows through the radiator. Hence, the fan performance needs to meet the requirements of large flow rate, high static pressure.

It is evaluated that the Reynolds number around the blades will be less than 10×10^5 when the fan is operated under extreme conditions. Michael S. Selig et al. reported that the Airfoils 30 can meet the demand of high

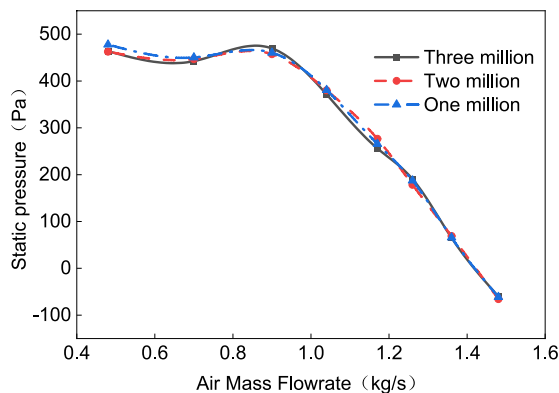


Fig. 3. Verification of mesh-independence.

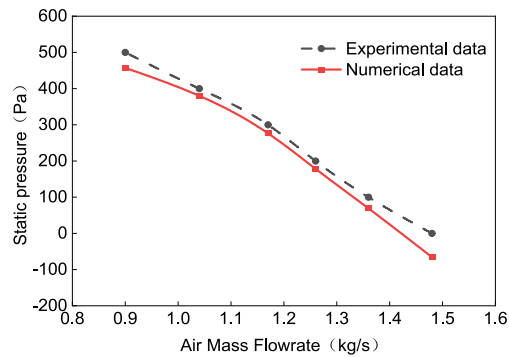


Fig. 4. Fan curve verification.

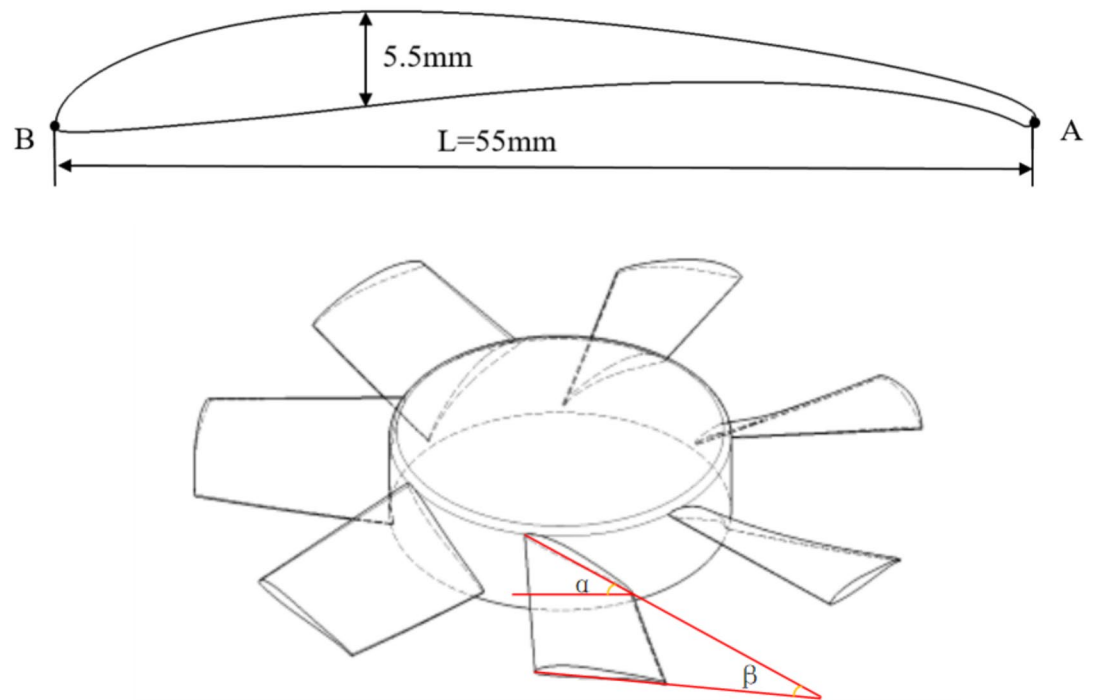


Fig. 5. Airfoil 30 profile and the configuration definition.

lift-to-drag ratio at low Reynolds number²⁸, and its profile is shown in the (Fig. 5). The relative thickness of this airfoil is 10%. The coordinates of the outer profile of the airfoil are listed in related file. The data in the attached table originates from point A along the upper edge to B and back to point A. This airfoil has a maximum lift coefficient of up to 2. And the lift-to-drag ratio does not vary significantly with angle of attack. Based on the helicopter cooling system and motor size constraints, and taking into account the motor cooling requirements, the diameter, hub ratio and the hub thickness of the fan is identified to be 300 mm, 0.43, and 40 mm, respectively. Then the effects of the fan torsion angle, chord length, mounting angle, and the number of blades on the performance of the fan will be investigated. The definition of the parameters mentioned above is shown in α is mounting angle. It is the angle between root chord line and the plane perpendicularly to the fan axial. β is torsion angle. It is the angle between chord line and the tip chord line. L is the chord length.

Optimization of torsion angle

In order to investigate the impacts of blade torsion angle on the performance of the fan, the torsion angles of 22, 24, 26, 28, and 30° were set for numerical calculations with a blade chord length of 55 mm, a number of blades of 7, a mounting angle of 39°, and a rotational speed of 4250 RPM (revolution per minutes), respectively. The flow rate of the fan is set to be 1.17 kg/s in the calculation. Because, the original fan experimental results show that as the air flow rate reaches 1.17 kg/s and above, it can meet the heat dissipation requirements of the radiator. The static pressure distribution on the blade is very important. It is a directly reflection of the fluid behaviour. Hence, it is used by scholars and valued results have been obtained^{10,26,27}. The relationships between the static pressure,

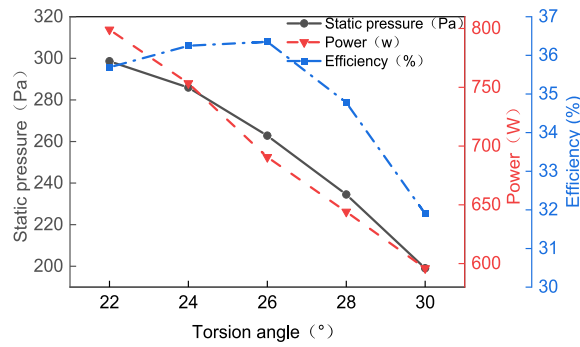
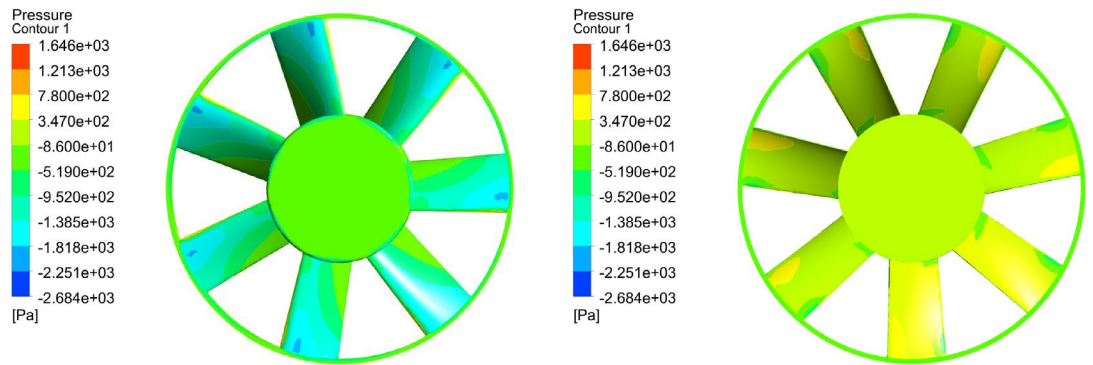
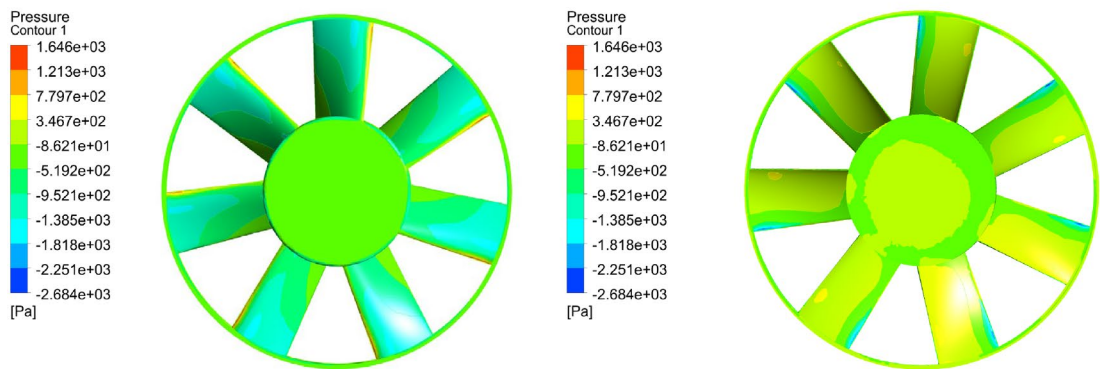


Fig. 6. Comparison of fan performance curves with different torsion angle.



(1) 22° torsion angle fan static pressure distribution diagram



(2) Static pressure distribution of fan with 30° torsion angle

Fig. 7. Comparison of static pressure of fans with different torsion angles.

power, efficiency and the torsion angle is shown in (Fig. 6). The static pressure and power decrease as the torsion angle increases. Because, as the torsion angle increase, less air will hit the blade directly, and smaller friction force will be generated. When the torsion angle is 26°, the fan efficiency is the highest. The pressure distribution on the blade surface is shown in (Fig. 7) as the torsion angles are set to be 22° and 30°, respectively. When the blade torsion angle is small, there is a large area of positive pressure zone on the blade pressure surface, and on the blade root and trailing edge exists a small negative pressure zone. There is an obvious pressure difference

on the blade pressure surface, and the pressure difference is the main driving force for the fan to push the air flowing. At the same time, there may be vortex near the negative and positive pressure junction zone. The vortex dominates fan power loss in practice. When the torsion angle is large, there is a large negative pressure area at the trailing edge of the blades, which leads to the significant vortex, causing low fan efficiency. In all, as the torsion angle is 26° , the highest efficiency is obtained. Meanwhile, the static pressure and the powerkeep in reasonable range.

The improvement of fan efficiency is a key measure for energy conservation and carbon reduction in UAV systems. The reason is twofold: firstly, a more efficient fan can reduce the fuel consumption of UAV engines. From the perspective of greenhouse effect, for every kilowatt hour of electricity saved by a fan, the corresponding reduction in CO_2 emissions is about 0.5 kg. Secondly, the improvement of fan efficiency can, in turn, lower the inlet temperature of the engine coolant and enhance the efficiency of the engine. It can reduce greenhouse gas emissions as well.

Chord length optimization

In order to investigate the effects of blade chord length on the fan performance, the chord lengths of 51, 53, 55, 57, and 59 mm are set for numerical calculations of fan performance at a blade torsion angle of 26° , a blade number of 7, a mounting angle of 39° , and a fan rotational speed of 4,250 RPM, respectively. The relationships between the static pressure, power, efficiency and the chord length of the fan is shown in (Fig. 8). The static pressure and power increase as the chord length increases. Because, as the chord length increases, the contact surface between the air and the blade surface becomes larger. The work done by the blades on the fluid increases, which in turn leads to an increase in the power and static pressure of the fan. The highest efficiency of the fan is achieved when the chord length is 55 mm as shown in (Fig. 8). Comparing the static pressure distributions of the fans with various chord lengths, they are extremely similar at two different chord lengths, as shown in (Fig. 9). The highest efficiency of the fan occurs as the chord length of the fan is 55 mm. It is probably due to the fact that the work consumed by friction accounts for a lower percentage of the total work. Although the low power is available, the static pressure is low also as the chord length is 51 mm and 53 mm. The low static pressure is not preferred for the fan performance in helicopter radiator system. Therefore, the chord length 55 mm of the fan is identified.

Mounting angle optimization

In order to investigate the impacts of blade mounting angle on the performance of the fan, the blade mounting angles of 35° , 37° , 39° , 41° , and 43° are numerically calculated for a blade torsion angle of 26° , a blade number of 7, a chord length of 55 mm, and a motor rotational speed of 4250 RPM, respectively. The relationships between the static pressure, power, efficiency and the installation angle of the fan are shown in (Fig. 10). The static pressure and power increase as the installation angle increases. Because, the effective work done by the blades on the fluid increases as the installation angle increases, which in turn leads to an increase in the power and static pressure of the fan. Similar phenomenon is observed as the chord length increases. The fan efficiency is the highest as the mounting angle is 39° . As shown in (Fig. 11), when the mounting angle is small, there is a high-pressure region at the leading edge of the blades and a low-pressure region at the trailing edge. The existed the high and low-pressure regions prompt the flow of air. However, the high and low-pressure regions close to the top of the blades may leads to backflow, which reduces the efficiency of the fan. When the mounting angle is larger, the back flow area significantly reduces and the fan efficiency increases, but the power is greater than the design value of 800 w. Therefore, the blade mounting angle of 39° is considered to be the optimal choice.

Optimization of the number of blades

In order to investigate the effects of number of blades on the performance of the fan, the number of blades set to 5,7,9 are numerically calculated for a blade torsion angle of 26° , mounting angle of 39° , chord length of 55 mm, and fan rotational speed of 4250 RPM (10% lower than the original one), respectively. The results calculated under various conditions are shown in (Fig. 12). As the number of blades increases, the efficiency, power and static pressure of the fan increases. It is clear from (Fig. 13), when the number of blades is 9, there is a more pronounced pressure difference on the blades, especially at the edge of the blades. The pressure difference may

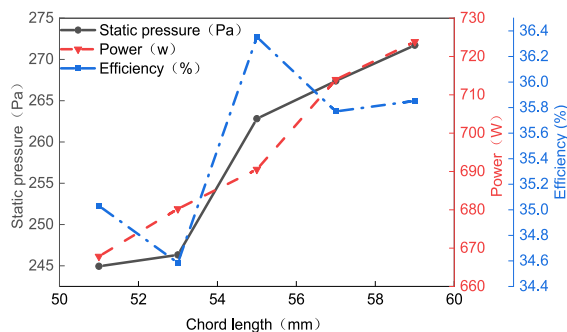
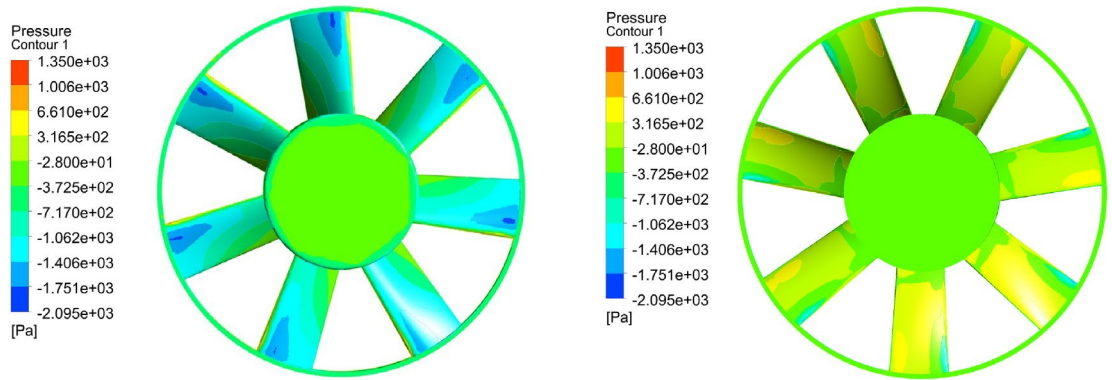
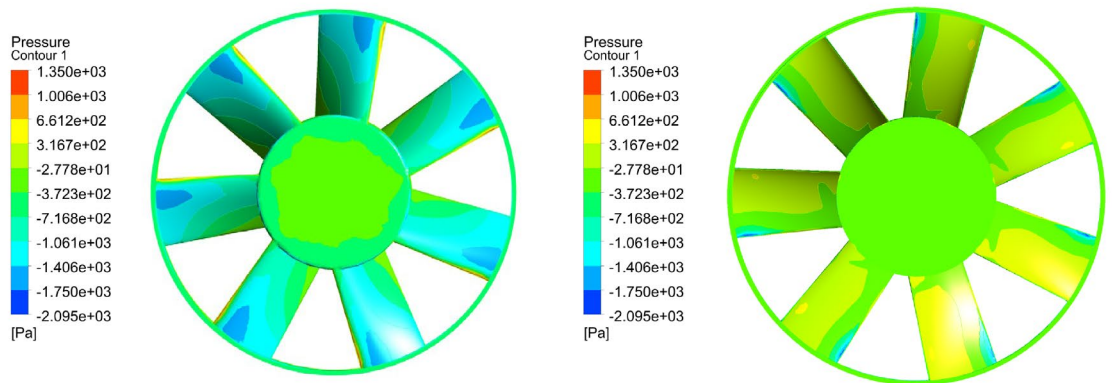


Fig. 8. Comparison of performance curves of fans with different chord lengths.



(1) Static pressure distribution of 51 mm chord length fan



(2) Static pressure distribution of 59 mm chord length fan

Fig. 9. Comparison of fan static pressure at different chord lengths.

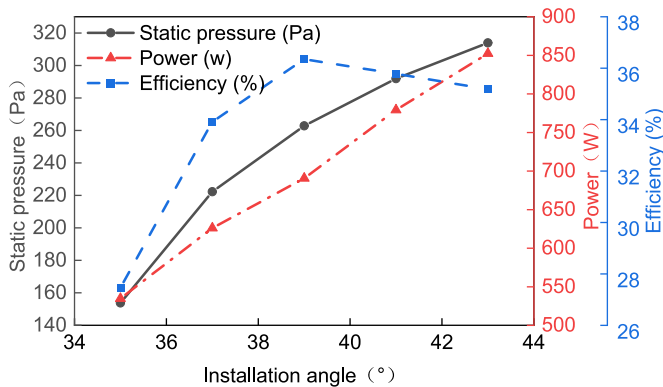
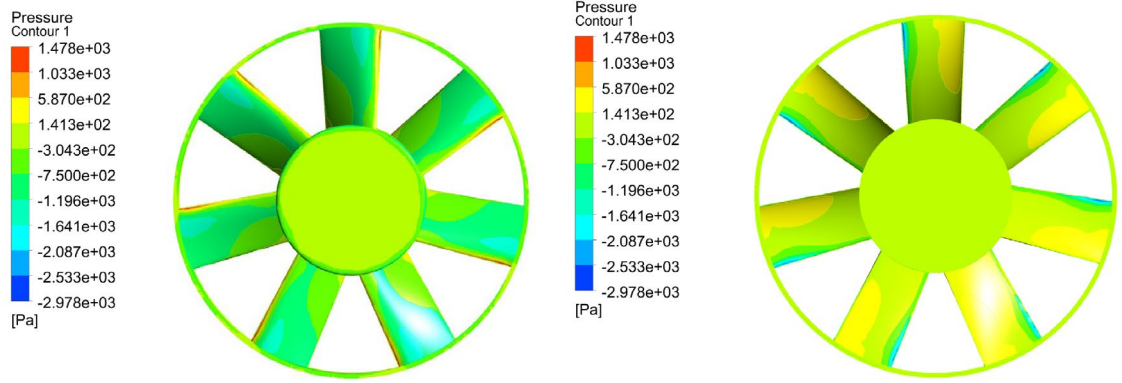


Fig. 10. Comparison of fan performance curves at different mounting angles.

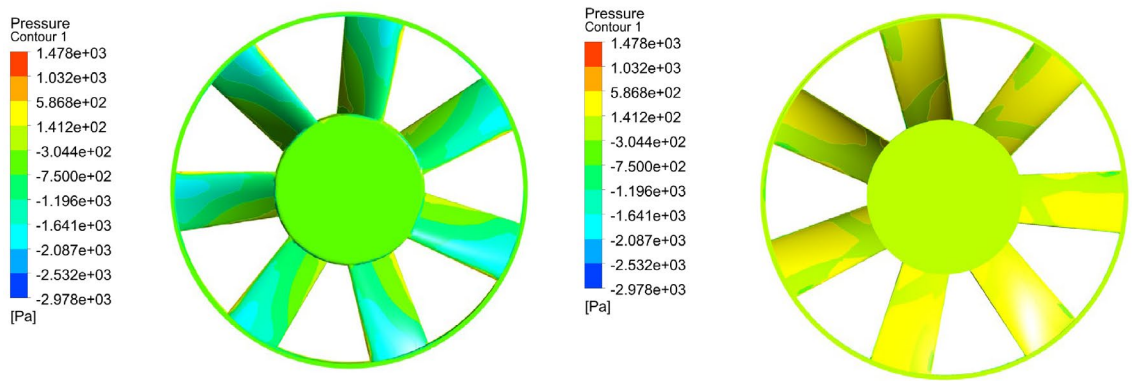
lead to back flow and reduce the efficiency of the fan. Considering the size and weight of the fan and the actual available power for the heat radiator system (max. 800 w), it is appropriate to choose a blade number of 7.

Identification of fan parameters

The key parameters of the fan have been investigated thoroughly. The optimized fan parameters are identified. The fan diameter is 300 mm. The diameter of the hub is 130 mm, and the Airfoils 30 model is scaled up to a chord length of 55 mm, a blade mounting angle of 39°, and a torsion angle of 26°. The simulation based on the



(1) Static pressure distribution of fan with 35° mounting angle



(2) Static pressure distribution of fan with 43° mounting angle

Fig. 11. Comparison of fan static pressure at different mounting angles.

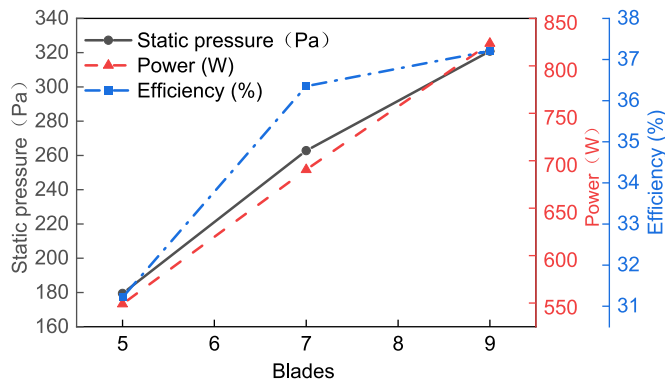
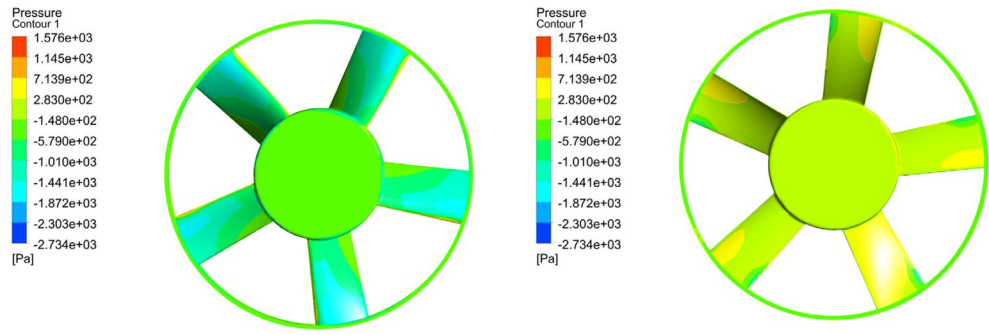
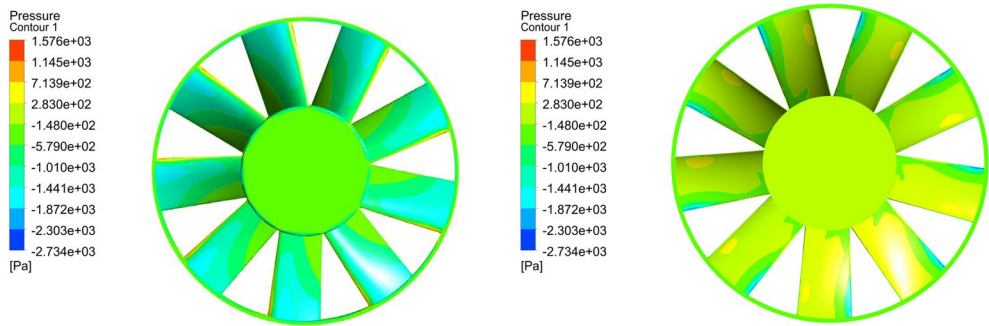


Fig. 12. Comparison of fan performance curves with different number of blades.

new fan is carried out based on the numerical model. The performance curve of the new fan is obtained at a fan speed of 4250 RPM and a fan flow rate of 1.17 kg/s. The performance curves of the new fan and the original fan are shown in (Fig. 14) below. The new designed fan performance improves significantly at high flow rates. The new designed fan can generate higher static pressure as compared to the original one at high flow rate (1.17 kg/s and above). The fan efficiency increases about 13.6%. The power consumption decrease about 9.5% (about 73



(1) Static pressure distribution of a 5-blade fan



(2) Static pressure distribution of a 9-blade fan

Fig. 13. Comparison of static pressure of fans with different number of blades.

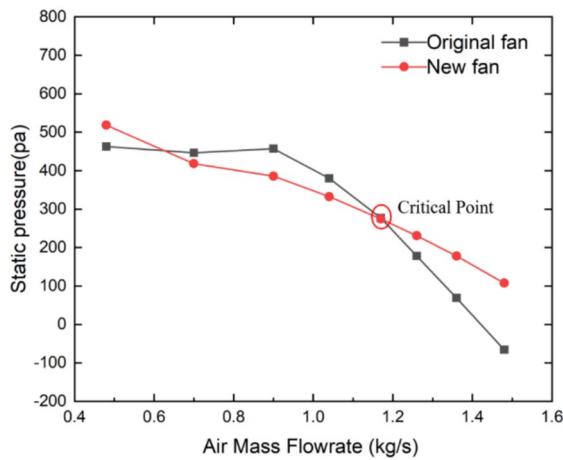


Fig. 14. Comparison of fan characterization curves.

W). The fan rotational speed decreases 10.5%. The improvement of fan efficiency is a key measure for energy conservation and carbon reduction in unmanned helicopter systems. The 73 W power consumption of the fan decrease indicates that 1.2 kg green-house gas emission reduces per day. The lower power consumption will result in a 0.14% cruising endurance increase.

The velocity distribution of the new designed fan is shown in (Fig. 15). The fluid velocity is small due to the viscous forces received by the air near the fan hub. Additionally, the air velocity increase gradually from the blade root to the tip. In addition, the tip of the fan blade is connected to the rotating mechanism, which avoids the generation of backflow at the tip of the blade.

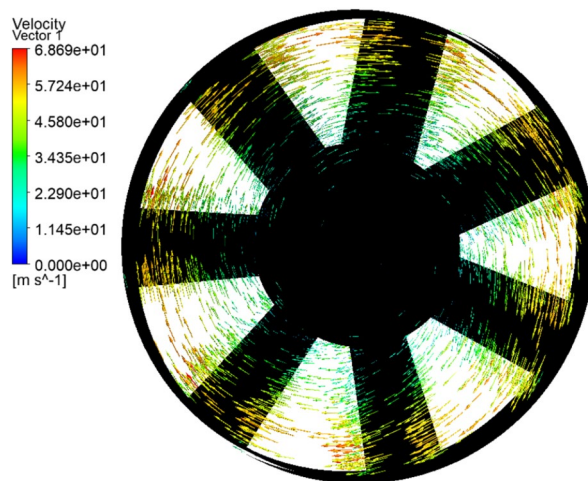


Fig. 15. Velocity distribution.

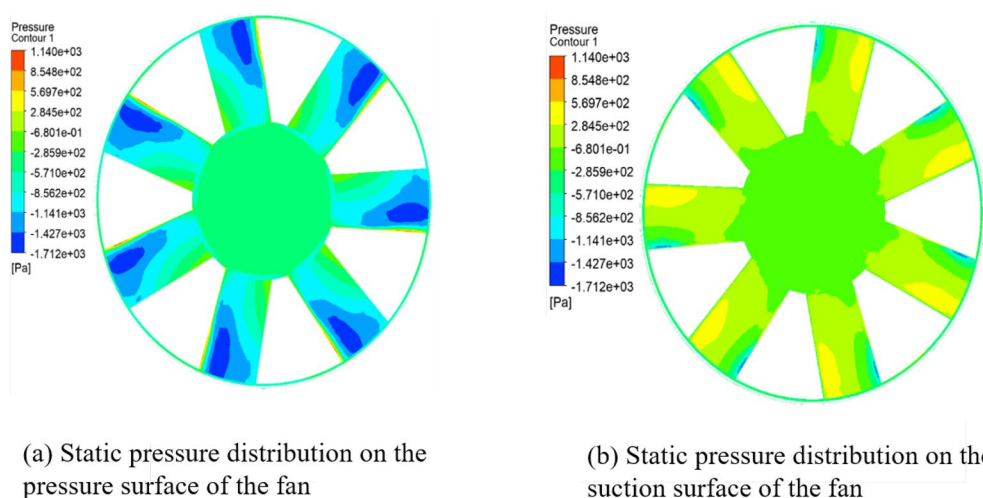


Fig. 16. Fan blade surface pressure distribution.

As shown in Fig. 16, the high pressure region of the pressure surface of the blade is the work area of the fan, which mainly drives the airflow moving. In addition, from the fan blade surface pressure surface distribution figures, the high static pressure region locates at the leading edge of the blade, and the low static pressure region mainly exists with the trailing edge of the fan blade. In general, the static pressure increases gradually along the radial direction of the fan.

Fan fabrication additive manufacturing technology

The CFD-optimized fan blade is twisted seriously, and the distribution of the blade airfoil is specific, so it is very difficult to ensure the blade accuracy and the surface finish fabricated by traditional machining process. However, it is easily to handle by additive manufacturing. It has been used in various areas and promising results have been obtained^{29–32}. The fan for this test is manufactured by the stereolithography additive manufacturing, and the material used is reinforced nylon. The manufacturing process is as follows.

The CAD software is adopted to design models. Large overhanging structure should be avoided during the manufacturing. The blade thickness should transit smoothly;

In order to keep the balance between printing speed and precision, the layer height is set approximately for 0.1 mm;

After printing, it is compulsory to perform the second time curing in the ultraviolet curing box. The curing temperature is maintained at 50 °C -60 °C;

The printed product has been polished to ensure that the fan surface is smooth enough. The printed fan is shown in (Fig. 17).

The simulation optimization of CFD and intelligent manufacturing form a digital twin driving relationship of “design production” integration. By conducting multi parameter virtual simulation and automatic optimization of



Fig. 17. Fan fabricated by additive manufacturing.

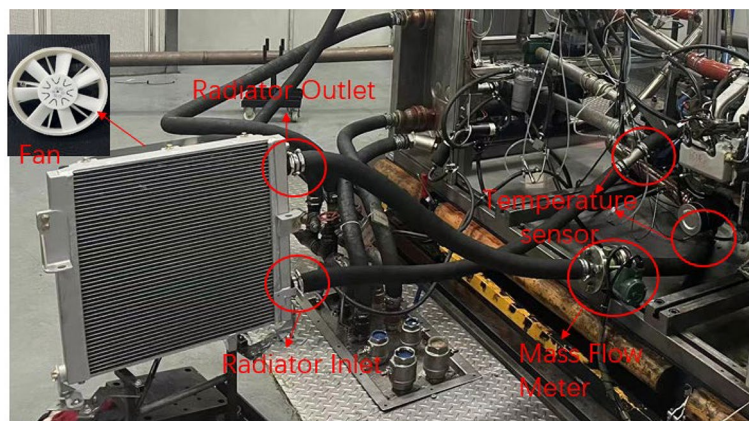


Fig. 18. Radiator test setup.

fan performance (such as aerodynamic efficiency and blade characteristics) through CFD, the optimal geometric configuration of the fan can be directly generated. These data become input instructions for autonomous manufacturing systems: the CFD optimized blade configuration can be directly converted into 3D printer manufacturing code, and the 3D printing system automatically optimizes the printing path based on the received code. This deep integration enables the production line to dynamically adjust manufacturing parameters based on the "performance optimal solution" provided by CFD, achieving efficient and precise manufacturing from batch production to customized products. While improving product performance consistency, it significantly reduces trial and error costs and energy consumption, forming a data-driven intelligent production loop. The data driven intelligent production has been widely used in electrical devices printing^{33–36}.

Experimental test

In order to test the performance of the newly designed fan, the maximum stable output power of the engine (90 kW) is selected as the target at room temperature of 40 °C and a fan power of 800W (the maximum power of the fan allowed by the helicopter avionics system).

In this experiment, the volume of testing room is about 30 m³, and it can be assumed that the external domain (with air-conditioning) can be treated as infinite heat sink. The testing room temperature is used to simulate the helicopter and radiator working temperature in practice at 40 °C. The setup is shown in (Fig. 18). The temperature sensors (accuracy ± 0.2 °C) are installed at the engine inlet and outlet locations to measure the temperature of the liquid, respectively. The flow rate of the liquid is measured by the liquid flow meter (± 0.1 kg/s). Air temperature sensors were used to measure the room temperature, which is controlled by the air-conditioning. The fan installed on the radiator envelop is used to cool down the coolant. The coolant is then used to remove the heat generated during the fuel burning in the cylinder. Hence, engine output power is inversely proportional to the coolant temperature. If a high engine output power (≥ 90 kW) can be maintained for at least 5 min, it can be deemed as successful design of the fan. During test, the ambient temperature is controlled at 40 °C by using the automatic closed-loop control air-conditioning, and the fan power is maintained at 690 W. The helicopter engine speed and power are gradually increases. The radiator inlet and outlet temperatures are monitored on-line (the permitted highest temperature is 110 °C). When the engine inlet and outlet temperature

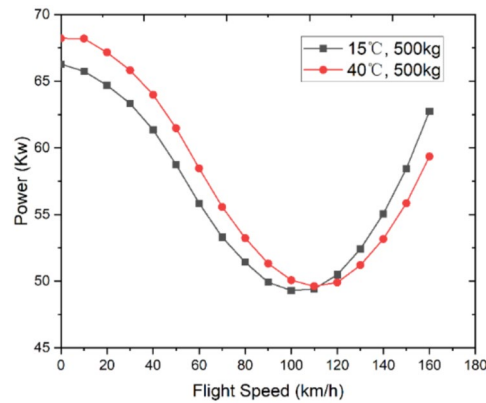


Fig. 19. Performance of the unmanned helicopter main rotor system (altitude 0 km).



Fig. 20. Fan installation on unmanned helicopter.

is stabilized, the liquid flow, engine power, fan power and ambient temperature are recorded. The engine power can be identified as the reading from the control panel keeps steady for 5 min.

The experimental results indicate that the maximum output power of the engine is over than 90 kW. The engine 90 kW output is a critical point in this project. Because it is a minimum value to keep the helicopter hovering indefinitely with 500 kg loading (maximum value for the system) under 40 °C. It is the criteria to identify the designing successful or not. The engine output power is inversely proportional to the coolant temperature. The permitted highest temperature of the coolant is 110 °C, which is identified by the coolant properties. The maximum engine output power obtained is a conservative value as the coolant temperature maintains at 110 °C. The higher engine output power (> 90 kW) can be obtained if the coolant temperature can be maintained lower than 110 °C as the air temperature is 40 °C. The helicopter performance curve with 500 kg load under various temperature is shown in (Fig. 19). The drag force of the helicopter is composed of parasitic drag force, induced drag force and airfoil drag force. The highest drag force of the helicopter system occurs as the helicopter is hovering. The same is truth in respect to the engine power. The maximum power requirement for the main rotor system is 68 Kw. The rate power of the avionics equipped on the unmanned helicopter system is approximately 2 Kw. The helicopter could hover for a long endurance with 500 kg loading under 40 °C.

The fan installation on the unmanned helicopter is shown in (Fig. 20). It fits the unmanned helicopter fuselage well.

Conclusions

This work systematically investigates the effects of blade torsion angle, chord length, mounting angle, and blade number on the performance of a compact cooling fan used for unmanned helicopters. The optimal configuration (26° torsion angle, 55 mm chord length, 39° mounting angle, 7 blades) is identified by using CFD simulations and validated in the lab. The fan efficiency increases about 13.6%, and the power consumption decrease about 9.5% (about 73 W), and the fan rotational speed decreases 10.5% as compared to the original one. Experimental

validation also confirm that the optimized fan enables engine output power larger than 90 kW under 40 °C conditions. It can ensure the Unmanned helicopter hovers indefinitely with a 500 kg payload under 40 °C conditions.

Beyond technical performance, this study highlights the sustainability benefits of integrating CFD with additive manufacturing. Improved fan efficiency contributes to lower fuel consumption and reduced greenhouse gas emissions in UAV systems, while additive manufacturing reduces trial-and-error costs and minimizes material waste. Most importantly, this work demonstrates how CFD-enabled design and additive manufacturing can form the basis of a cyber-physical production framework. By directly linking optimization results with manufacturing instructions, this approach establishes a closed-loop paradigm of simulation-driven intelligent production. Such integration has strong potential for extension to CFD-based fan design, real-time process monitoring, and adaptive control in additive manufacturing.

In conclusion, the research not only advances UAV cooling system design but also contributes to the broader goals of autonomous, sustainable manufacturing, aligning directly with the objectives of the Additive Manufacturing for Sustainable Industry initiative.

Data availability

The datasets generated and analyzed during the current study are available from the corresponding author on reasonable request.

Received: 2 November 2025; Accepted: 8 January 2026

Published online: 17 January 2026

References

- Shuhong, L. I. U., Yulin, W. U. & Zhigang, Z. U. O. *Applied Fluid Mechanics* (Tsinghua University Press, 2012) ((In Chinese)).
- Moreau, S. Improvement of fan design using CFD. SAE Technical Paper 970934, (2002).
- Henner M. Kessaci S. Moreau S. Latest improvements of CFD Models of engine cooling axial fan systems. SAE Technical Paper Series.
- Yi-You, W., Min, W. U., Dun-Lu, L. Noise Calculation of engine cooling fan based on CFD. *Mechan. Eng.* (2009).
- Wang, A., Hui, X. Z. & Ghazialam, H. *Evaluation of the Multiple Reference Frame (MRF) Model in a Truck Fan Simulation* (SAE Paper, 2005).
- Ota, H. et al. *Development of High Efficient Radiator Cooling Fan for Automotive Application* (SAE Technical Paper, 2013).
- Kobayashi, Y., Kohri, I. & Matsushima, Y. *Study of Influence of MRF Method on the Prediction of the Engine Cooling Fan Performance* (SAE Technical Paper, 2011).
- Kohri, I., Kobayashi, Y. & Matsushima, Y. Prediction of the performance of the engine cooling fan with CFD simulation. *SAE Int. J. Passenger Cars-Mechan. Syst.* **3**, 508–522 (2010).
- Yuntao, C. *CFD Analysis and Low Noise Optimization Design of Engine Cooling Fan for Sedan* (Jilin University, 2007) ((In Chinese)).
- Xingrong, W. *CFD Analysis and Simulation Process Optimization of Engine Cooling Fan Aerodynamic Performance* (South China University of Technology, 2013) ((In Chinese)).
- Shengfu, Li. & Xinxin, W. Optimization design analysis of automotive cooling fan blade parameters. *Mechan. Design Manuf.* **07**, 48–52 (2019) ((In Chinese)).
- Yaozhen, Z. *CFD Analysis and Low Noise Optimization Design of Car Engine Cooling Fan* (Jilin University, 2007) ((In Chinese)).
- Wang, Z.N., Wang, H. Design of automobile cooling fan based on computational fluid dynamics. Optimized design of automobile cooling fan based on computational fluid dynamics. *Mechanical Design and Manufacturing*, 2016 (10): 182–186
- Wang, Y., Lu J., Jiang, B., et al. Study on the effect of blade inclination on the performance of cross-flow wind turbine using CFD technology. *Journal of Hefei University of Technology: Natural Science Edition*, (2012). (In Chinese)
- Li, Y. E., Feng, X. U., Yan, S. H. I., Haibo, L. I. N. & Chao, S. U. N. Research and optimization of aerodynamic performance of automobile engine cooling fan. *Pract. Energy Saving Technol.* **5**, 76–80 (2018) ((In Chinese)).
- Tang Zhao. Research and optimization of engine cooling fan blade parameters. Guangzhou: South China University of Technology, (2012). (In Chinese)
- Jung, Y. S., Lee, B. & Baeder, J. Prediction of Coaxial rotor hub flow using mercury framework. *J. Am. Helicopter Soc.* **69**(2), 1–4 (2024).
- Renaud, T., Pape, A. L. & Péron, S. Numerical analysis of hub and fuselage drag breakdown of a helicopter configuration. *CEAS Aeronaut. J.* **4**(4), 409–419 (2013).
- Zaharia, S. M. et al. Material extrusion additive manufacturing of the composite UAV Used for search-and-rescue missions. *Drones* **7**, 602 (2023).
- Helge, K. et al. Additive manufacturing of porous structures for unmanned aerial vehicles applications. *Adv. Eng. Mater.* **20**, 1800290 (2018).
- Bozkurttas, M. et al. *CFD-Based Analysis and Design of Biomimetic Flexible Propulsor for Autonomous Underwater Vehicles* (AIAA, 2007).
- Zhao, J. et al. *CFD analysis of Ducted-Fan UAV Based on Magnus Effect* (IEEE, 2012).
- Yin, S. et al. Electric Scissors for precise generation of organic droplets in microfluidics: a universal approach that goes beyond surface wettability. *J. Phys. Chem. C* **123**, 25643 (2019).
- Yin, S. et al. Triple-layered encapsulation through direct droplet impact. *J. Colloid Interface Sci.* **615**, 887 (2023).
- VA113-BBL504P fan performance experiment report.
- Subramanya, R. *Modelling and Simulation of Fan Performance Using CFD Group* (Linköping University, 2020).
- Zhang, S., et al. Intelligent simulation and optimization of axial flow fan based on CFD. (2023).
- Low Reynolds Number, Low drag, high lift airfoil. Michael S. Selig, William Holmes, Frank Stauder. Patent.
- Ding, D., Ng, B. E., Liu, H., Lu, X. & Wan, M. P. The characteristics and formation mechanism of emissions from thermal decomposition of 3D printer polymer filaments. *Sci. Total Environ.* **20**, 984–994 (2019).
- Zhang, H. & Moon, S. K. Hybrid machine learning method to determine the optimal operating process window in aerosol jet 3D printing. *ACS Appl. Mater. Interface* **11**, 17994–18003 (2019).
- Zhang, H., Moon, S. K. & Ngo, T. H. 3D printed electronics of non-contact ink writing techniques: status and promise. *Int. J. Precis. Eng. Manuf. Green Technol.* **7**, 511–524 (2020).
- Yang, X. et al. Active fabrics with controllable stiffness for robotic assistive interface. *Adv. Mater.* **36**, 2404502 (2024).
- Zhang H, Moon SK, Ngo TH, Tou J, Mohamed AB. A hybrid machine learning approach for the quality optimization of a 3D printed sensor. In *2018 International Conference on Intelligent Rail Transportation (ICIRT)*. IEEE.

34. Li, M., Yin, S., Liu, Z. & Zhang, H. Machine learning enables electrical resistivity modeling of printed lines in aerosol jet 3D printing. *Sci. Rep.* **14**, 14614 (2024).
35. Wang, B. et al. A post-treatment method to enhance the property of aerosol jet printed electric circuit on 3D printed substrate. *Materials* **13**, 5602 (2020).
36. Zhang, H., Huang, J., Zhang, X. & Wong, C. N. Autonomous optimization of process parameters and in-situ anomaly detection in aerosol jet printing by an integrated machine learning approach. *Additive Manuf* **86**, 104208 (2024).

Acknowledgements

This research was supported by the Anhui HAERY Aviation Power Co., Ltd. This work was also supported by the Technology development Program (No.RS-2025-25443487) funded by the Ministry of SMEs and Startups (MSS, Korea).

Author contributions

Liang Si: Conceptualization, Methodology, Investigation, Writing original draft. Zhixin Liu: Conceptualization, Methodology, Investigation, Writing original draft. Nannan Xiao: Methodology, Investigation, Writing original draft. Yuwen Zhang: Methodology, Investigation, Writing original draft. Yebao Liu: Methodology, Writing original draft, Writing. Shuai Deng: Methodology, Writing original draft. Yuchuan Li: Methodology, Writing original draft. Haisheng Yang: Validation, Writing original draft. Xiongjian Zhang: Validation, Writing original draft. Guoqiang Fu; - review & Editing draft. Joon Phil Choi: Methodology, Writing—review & editing.

Funding

This research was supported by the Anhui province fundamental research funding (No. 2024AH051814). Valuable support from Anhui HAERY Aviation Power Co., Ltd. This work was also supported by the Technology development Program (No.RS-2025-25443487) funded by the Ministry of SMEs and Startups (MSS, Korea).

Declarations

Competing intertests

The authors declare that they have no competing interest.

Additional information

Correspondence and requests for materials should be addressed to Z.L. or J.P.C.

Reprints and permissions information is available at www.nature.com/reprints.

Publisher's note Springer Nature remains neutral with regard to jurisdictional claims in published maps and institutional affiliations.

Open Access This article is licensed under a Creative Commons Attribution-NonCommercial-NoDerivatives 4.0 International License, which permits any non-commercial use, sharing, distribution and reproduction in any medium or format, as long as you give appropriate credit to the original author(s) and the source, provide a link to the Creative Commons licence, and indicate if you modified the licensed material. You do not have permission under this licence to share adapted material derived from this article or parts of it. The images or other third party material in this article are included in the article's Creative Commons licence, unless indicated otherwise in a credit line to the material. If material is not included in the article's Creative Commons licence and your intended use is not permitted by statutory regulation or exceeds the permitted use, you will need to obtain permission directly from the copyright holder. To view a copy of this licence, visit <http://creativecommons.org/licenses/by-nc-nd/4.0/>.

© The Author(s) 2026